Direct observation of fault zone structure at the brittle-ductile transition along the Salzach-Ennstal-Mariazell-Puchberg fault system, Austrian Alps

Erik Frost,[1,2] James Dolan,[1] Lothar Ratschbacher,[3] Bradley Hacker,[4] and Gareth Seward[4]

Received 21 May 2010; revised 27 October 2010; accepted 9 December 2010; published 17 February 2011.

[1] Structural analysis of two key exposures reveals the architecture of the brittle-ductile transition (BDT) of the subvertical, strike-slip Salzachtal fault. At Lichtensteinklamm, the fault zone is dominantly brittle, with a ~70 m wide, high-strain fault core highlighted by a 50 m thick, highly foliated gouge zone. In contrast, at Kitzlochklamm, deformation is dominantly ductile, albeit with relatively low strain indicated by weak lattice-preferred orientations (LPOs). The marked contrast in structural style indicates that these sites span the BDT. The close proximity of the outcrops, coupled with Raman spectroscopy indicating similar maximum temperatures of ~400°C, suggests that the difference in exhumation depth is small, with a commensurately small difference in total downdip width of the BDT. The small strains indicated by weak LPOs at Kitzlochklamm, coupled with evidence for brittle slip at the main fault contact and along the sides of a 5 m wide fault-bounded sliver of Klammkalk exposed 30 m into the Grauwacken zone rocks, suggest the possibility that this exposure may record hybrid behavior at different times during the earthquake cycle, with ductile deformation occurring during slow interseismic slip and brittle deformation occurring during earthquakes, as dynamic coseismic stresses induced a strain rate–dependent shift to brittle fault behavior within the nominally ductile regime in the lower part of the BDT. A key aspect of both outcrops is evidence of a high degree of strain localization through the BDT, with high-strain fault cores no wider than a few tens of meters.

Citation: Frost, E., J. Dolan, L. Ratschbacher, B. Hacker, and G. Seward (2011), Direct observation of fault zone structure at the brittle-ductile transition along the Salzach-Ennstal-Mariazell-Puchberg fault system, Austrian Alps, *J. Geophys. Res.*, *116*, B02411, doi:10.1029/2010JB007719.

1. Introduction

[2] Knowledge of the structure and mechanics of fault zones at the brittle-ductile transition is vital to our understanding of the rheological characteristics of the base of the seismogenic zone, where many large earthquakes nucleate. Field and experimental studies have shown that, rather than being a simple transition from brittle faulting to ductile creep, this part of the crust can deform by a wide range of mechanisms dependent upon pressure, temperature, strain rate, grain size, fluid activity, mineralogy, phase transformations, and microstructure [e.g., *Tullis and Yund*, 1977, 1992; *Carter and Kirby*, 1978; *Sibson*, 1980, 1982; *Passchier*, 1982; *Hobbs et al.*, 1986; *Rutter*, 1986; *Janecke and Evans*, 1988; *Scholz*, 1988; *Shimamoto*, 1989; *Hacker and Christie*, 1990; *Chester*, 1995; *White*, 1996; *Hacker*, 1997; *Montesi and Hirth*, 2003; *Shigematsu et al.*, 2004; *Lin et al.*, 2005].

[3] In one widely accepted model of the structure and mechanics of faulting in the crust [*Scholz*, 2002], deformation mechanisms change across the brittle-ductile transition from cataclastic flow to crystal-plastic flow concurrent with the onset of interseismic quartz plasticity at ~300°C. The resulting interpretation is that the seismogenic crust deforms via frictional sliding, with strength increasing into the middle of the brittle-ductile transition (BDT). In the mid-BDT to lower BDT, strength begins to decrease as the crust deforms via temperature-controlled flow. Assuming a constant lithology, this model also suggests that faults narrow downward toward the brittle-ductile transition, and then gradually widen in the lower brittle-ductile transition as discrete slip surfaces disappear. Solution creep is expected to operate at all depths [*Brace and Kohlstedt*, 1980; *Sibson*, 1984; *Chester*, 1995], reducing fault strength compared to the traditional two-mechanism model.

[1]Department of Earth Sciences, University of Southern California, Los Angeles, California, USA.
[2]Now at Fugro William Lettis and Associates, Valencia, California, USA.
[3]Tektonophysik–Institut für Geowissenschaften, Technische Universität Bergakademie Freiberg, Freiberg, Germany.
[4]Department of Earth Science, University of California, Santa Barbara, California, USA.

0148-0227/11/2010JB007719

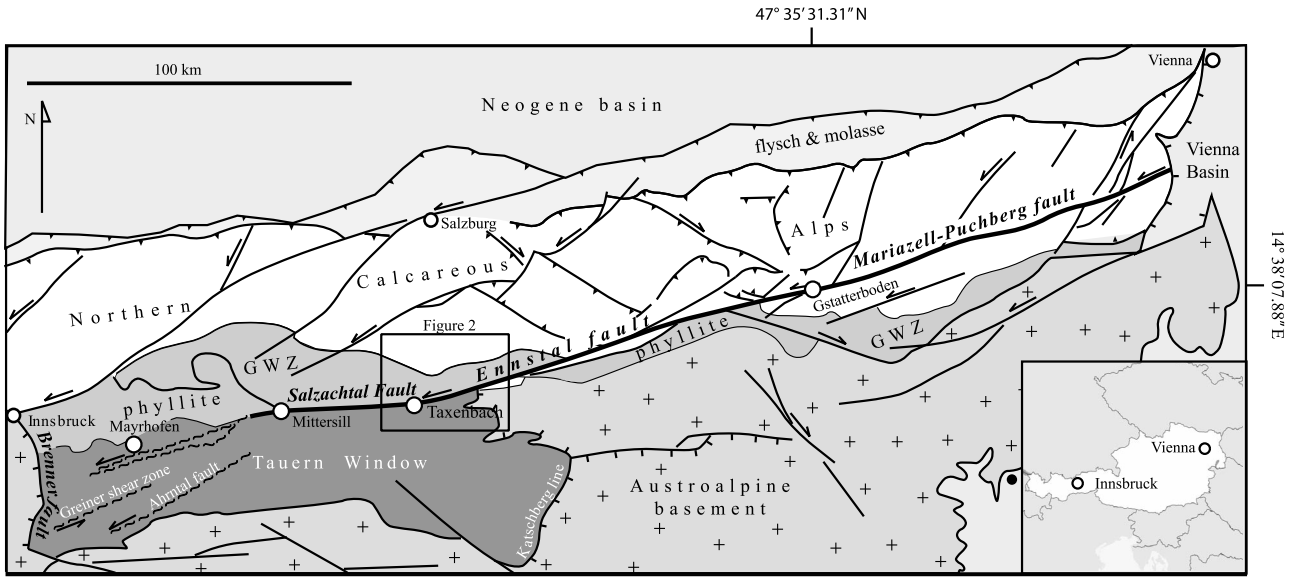

Figure 1. The Salzach-Ennstal-Mariazell-Puchberg (SEMP) fault zone and major structural features of the Eastern Alps [after *Linzer et al.*, 2002; after *Cole et al.*, 2007]. Differential exhumation of the fault exposes a range of exhumation depths along strike, from ductile shear zones in the Tauern Window, to brittle-ductile outcrops near Taxenbach, and finally brittle fault zones of decreasing exhumation depth to the east. Our study sites are located near Taxenbach, exposing the eastern end of the Salzachtal fault segment. A location map of our study area is provided in Figure 2.

[4] This study presents direct observations of a strike-slip fault exhumed from the brittle-ductile transition which, together with companion studies at shallower and deeper exhumation levels, allows insights that refine models of fault behavior throughout the crust [*Cole et al.*, 2007; *Frost et al.*, 2009]. The unique opportunity to directly observe depth-dependent changes on a single fault is afforded by the Salzach-Ennstal-Mariazell-Puchberg (SEMP) fault zone in central Austria. The SEMP fault zone has been differentially exhumed along strike, exposing a range of exhumation depths from near-surface conditions in the Vienna basin in the east to fully ductile middle crust in the western Tauern Window [*Ratschbacher et al.*, 1991a, 1991b]. The differential exhumation along strike resulted from westward increasing north-south shortening across the Eastern Alps; combined with subsidence in the easternmost Eastern Alps and the Pannonian basin, the entire SEMP fault zone was tilted eastward. Fault structures transition eastward from dominantly ductile to dominantly brittle around the northeast corner of the Tauern Window, providing a natural laboratory in which to evaluate models of fault behavior around the brittle-ductile transition.

2. Geologic Setting

[5] The SEMP fault is primarily a sinistral strike-slip fault zone that extends for 400 km across the Eastern Alps (Figure 1) [*Ratschbacher et al.*, 1991a, 1991b; *Linzer et al.*, 2002]. From west to east, the Salzachtal fault forms the northern boundary of the Tauern Window (exposing European and oceanic (Penninic) units beneath African (Austroalpine) units), the Ennstal fault forms the boundary between the central part of the Northern Calcareous Alps and the basement of the Austroalpine unit, and the Mariazell-Puchberg fault cuts across the southern margin of the eastern Northern Calcareous Alps, part of the Austroalpine cover. Structural and kinematic analysis of the southernmost nappe boundaries of the Northern Calcareous Alps [*Ratschbacher et al.*, 1991a, 1991b; *Decker et al.*, 1994; *Linzer et al.*, 1995] demonstrates that the individual segments of the SEMP constitute a throughgoing sinistral fault that accommodated north-south shortening and orogen-parallel extension. Geochronology within the Tauern Window and the ages of intraorogenic basins constrain the age of this deformation as Oligocene and Miocene [e.g., *Linzer et al.*, 2002].

3. Outcrop Description

[6] The Salzachtal fault forms the northeastern border of the Tauern Window. From west to east, this segment of the SEMP represents the transition from dominantly ductile deformation in the Ahorn shear zone within the Tauern Window [*Rosenberg and Schneider*, 2008] and ductile/ductile-brittle deformation in the Rinderkarsee shear zone at the edge of the Tauern Window [*Cole et al.*, 2007] to dominantly brittle deformation in the Ennstal segment (along the northern edge and to the east of the Tauern Window). Our study area is at the eastern end of the Salzachtal fault, where the fault zone is exposed in a pair of deeply incised, narrow gorges, Kitzlochklamm and Lichtensteinklamm, which are ~18 km apart (Figure 2). Along this part of the SEMP, the fault juxtaposes slates and phyllites of the Grauwacken zone of the Upper Austroalpine unit to the north against graphite-rich marbles tectonites (Klammkalk) of the Lower Austroalpine Nordrahmenzone [*Wang and Neubauer*, 1998]. The total displacement along this section of the fault has been estimated at 60 km on the basis of offset

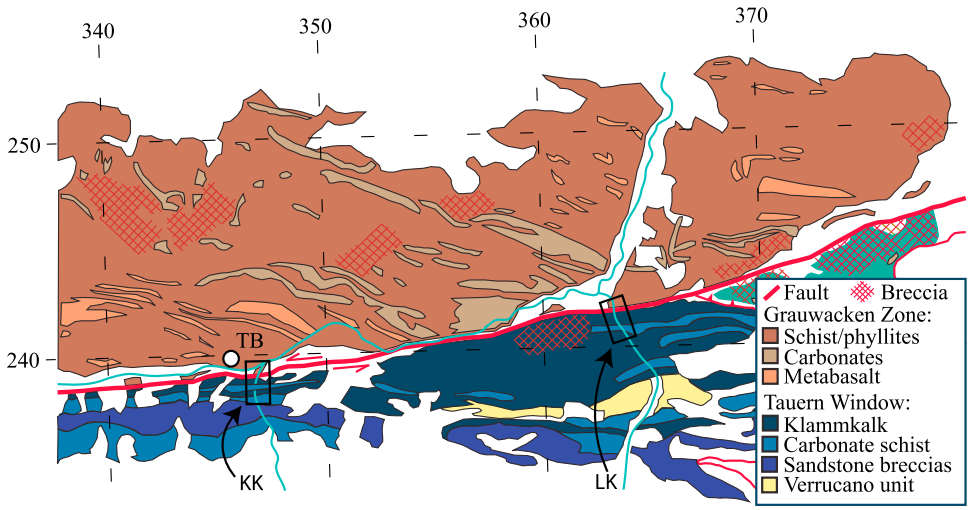

Figure 2. Simplified geologic map of study areas, redrafted from *Pestal and Hejl* [2005]. Grid markings (10 × 10 km) show universal transverse Mercator coordinates (WGS84, Zone 33). The SEMP juxtaposes Grauwacken zone rocks to the north against Klammkalk of the Tauern Window to the south. White areas on the map indicate Quaternary units, glacial cover, and vegetated land lacking outcrop. Lichtensteinklamm (LK) and Kitzlochklamm (KK) cut through units on both the north and south of the SEMP, providing natural fault-normal transects in which to study fault structure at this exhumation level. Taxenbach (TB) is indicated for reference.

of the Grauwacken zone units to the east [*Linzer et al.*, 1997, 2002].

3.1. Kitzlochklamm

[7] The outcrop at Kitzlochklamm provides 650 m of continuous, fault-normal exposure. The Grauwacken zone north of the fault, which is well exposed for a fault-normal distance of 200 m in the wide bed of the Rauriser River, comprises intercalated centimeter- to meter-thick intervals of graphite schist, carbonate schist, mica schist, and chlorite schist in order of decreasing abundance (Figure 3a). The Grauwacken zone is characterized by a well-developed S-C fabric adjacent to the fault (Figures 4a and 4b), a feature common to metapelites in the area [*Wang and Neubauer*, 1998]. The S-surfaces result from the alignment of platy minerals and dip steeply to moderately north-northeast, paralleling the original schistosity formed during earlier deformation [*Bickle and Hawkesworth*, 1978; *Exner*, 1996; *Kurz et al.*, 1996; *Wang and Neubauer*, 1998]. The C-surfaces range from millimeter- to centimeter-scale shear zones (Figures 3b and 3c), with the dominant set dipping steeply to the north and south, subparallel to the main fault. A small subset of the C-surfaces dips moderately northwest (Figure 4). Carbonate veins occur throughout the outcrop, and are commonly sheared and boudinaged (Figure 3b). Additional exposures to the north at a fault-normal distance of ~600 m lack well-developed shear zones and contain fewer veins. This provides an upper bound on the width of fault-related deformation in the Grauwacken zone north of the fault.

[8] The Klammkalk unit, exposed south of the fault, is composed primarily of a fine-grained, graphite-rich marble tectonite with local meter-scale lenses of chlorite schist. This unit is much more resistant than the Grauwacken zone, and the river creates a narrow, deeply incised gorge in the Klammkalk (Figure 5a). An S-C fabric is only weakly developed in the Klammkalk, which lacks the platy minerals in the Grauwacken zone rocks (Figure 4c). As a result, S-surfaces are weaker and less abundant than in the Grauwacken zone rocks. C-surfaces are present in two main sets, with one set dipping steeply north and south, subparallel to the main fault, the other dipping moderately northwest and southeast. C-surfaces are found throughout the 450 m of fault-normal exposure of the Klammkalk, albeit at a lower frequency than in the Grauwacken zone. Carbonate veins are ubiquitous, and most are sheared and boudinaged (Figure 5b). No change in macroscopic deformation style can be observed throughout the 450 m fault-normal width of the outcrop.

[9] With the exception of one fault-bounded, 5 m thick layer of Klammkalk that has been slivered off 30 m into the Grauwacken zone, the two units are sharply juxtaposed at the fault contact. This fault contact, which is well exposed, is a sharply defined, millimeter- to centimeter-scale zone devoid of gouge in which the Klammkalk is juxtaposed directly against graphite schist of the Grauwacken zone (Figure 5c). In contrast to the rest of the Grauwacken zone schists, which are mostly continuous along strike, the graphite schist within 10s of cm of the Klammkalk is heavily damaged, consisting of phacoids of schist up to 10 cm long with polished facets embedded in an anastomozing network of shear zones.

3.2. Lichtensteinklamm

[10] Lichtensteinklamm exposes the Salzachtal fault in the same lithologic units as at Kitzlochklamm. High water restricts access into the Klammkalk unit to a 150 m long, fault-normal transect. Grauwacken-zone rocks crop out in

Figure 3. (a) The Grauwacken zone at Kitzlochklamm, which is composed of alternating units of carbonate schist, mica schist, chlorite schist, and graphite schist, is well exposed for a fault-normal distance of 200 m in the bed of the Rauriser River. C-surfaces range from (b) millimeter-scale seams to (c) centimeter-scale shear zones.

riverbed exposures for 20 m adjacent to the fault, with additional outcrops 50 m north of the fault contact. Grauwacken zone rocks are exposed semicontinuously for several hundred meters north of the gouge zone in cut banks associated with parking lots and road construction east of the river.

[11] When comparing deformation at each Klamm, a major difference in structure is readily apparent. The

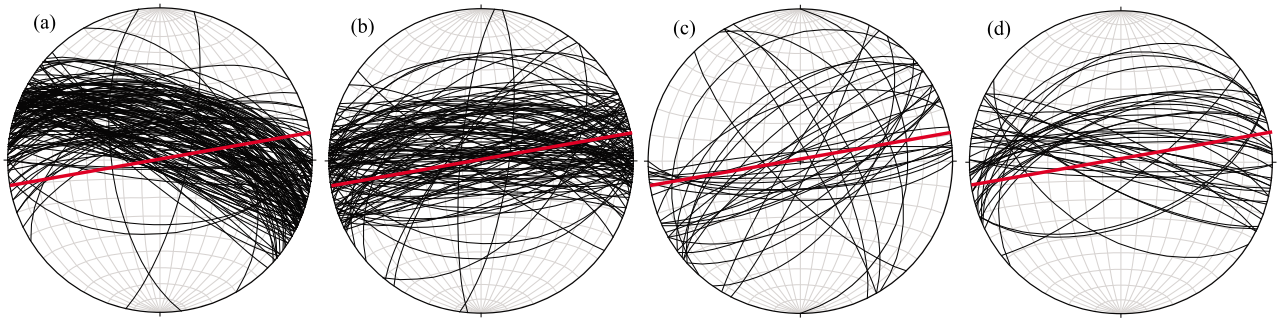

Figure 4. Grauwacken zone rocks at Kitzlochklamm display a well-developed S-C fabric common to metapelites in this area [*Wang and Neubauer*, 1998]. Red lines show the average strike of the SEMP in this region, as well as the strike of the gouge zone at Lichtensteinklamm. (a) The dominant set of S-surfaces dip steeply to moderately NNE, whereas (b) the C-surfaces tend to dip steeply north or south, with a second set of planes dipping moderately NW. (c) The Klammkalk unit lacks platy minerals but still contains a number of C-surfaces, with one set dipping steeply north and south and the other set dipping NW and SE. (d) C-surfaces measured in the Klammkalk at Lichtensteinklamm are broadly similar to those found at Kitzlochklamm, with a number of shear zones paralleling the SEMP (i.e., dipping steeply north to NNW/S and dipping SSE).

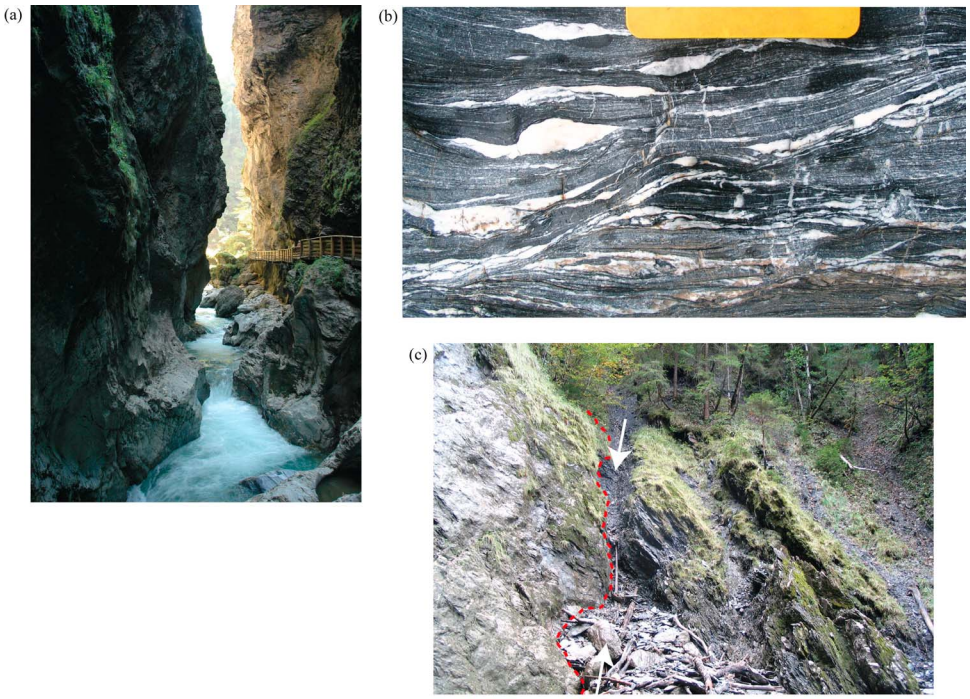

Figure 5. (a) The resistant Klammkalk at Kitzlochklamm forms a narrow, subvertical-walled gorge with deep, fast-moving water flowing through it. (b) Carbonate veins are found throughout the Klammkalk and are commonly sheared and boudinaged. (c) The fault contact juxtaposes Klammkalk (on the left) against Grauwacken zone (on the right) along a razor-sharp contact.

Grauwacken zone in the interval 20–50 m from the fault at Lichtensteinklamm has been ground into a fine-grained clay (Figure 6b). The clay is only locally exposed, and most typically has been remobilized by water and flowed downslope, such that our measurement of the width of the gouge zone is a maximum. In situ exposures of gouge display a vertical foliation but do not have a well-developed S-C fabric. Rather, the gouge exhibits distinct Riedel shears, most clearly visible in the chlorite-rich layers, consistent with left-lateral slip.

[12] Beyond the gouge zone, Grauwacken zone outcrops in the parking lots lack ductile shear zones and the extensive veining seen at Kitzlochklamm. Rather, these Grauwacken zone outcrops 100s of meters from the fault at Lichten-

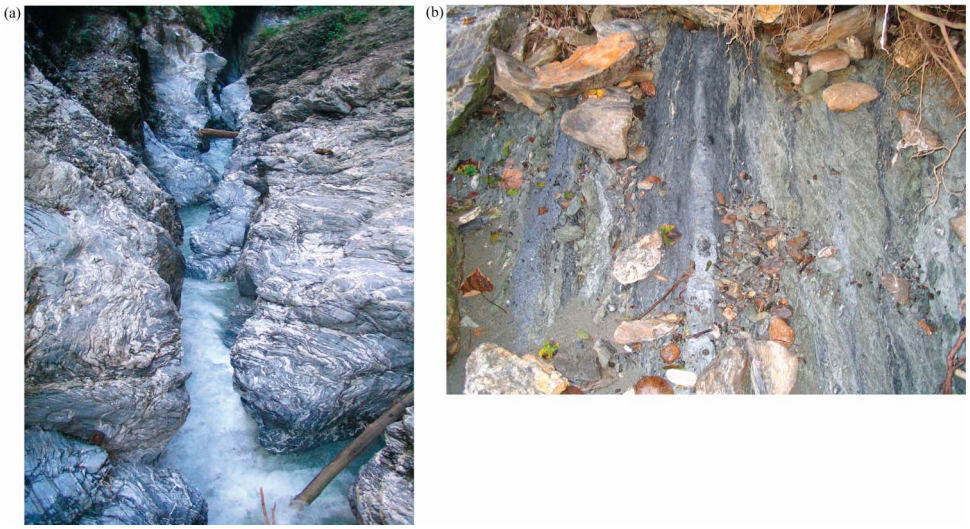

Figure 6. (a) The gorge at Lichtensteinklamm is much narrower than that at Kitzlochklamm, and the Klammkalk is pervasively veined. (b) The Grauwacken zone within 50 m of the fault contact has been gouged into a fine-grained clay. In situ exposures exhibit left-lateral Riedel shears, rather than the S-C fabric found at Kitzlochklamm. Pebbles and cobbles evidenced in photo are surficial stream deposits unrelated to clay gouge.

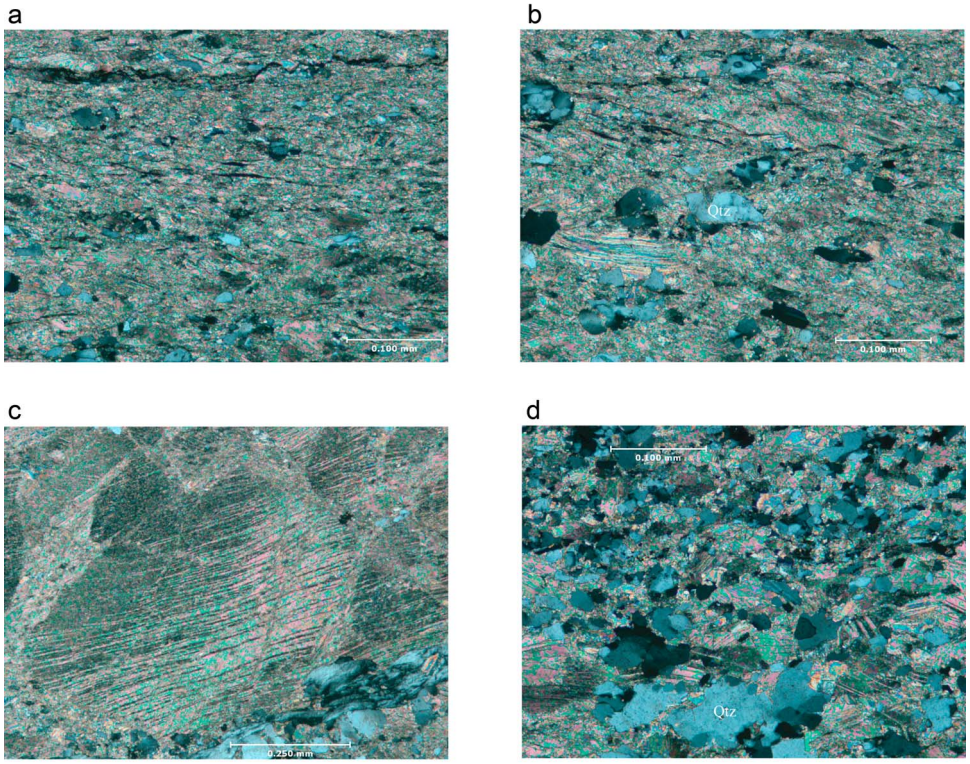

Figure 7. (a) Representative section of Kitzlochklamm Klammkalk, showing range of calcite grain sizes (sample 8216B1). (b) Vein calcite twins, type 3–4, sample 8216B1, Kitzlochklamm Klammkalk. (c) Quartz grains in sample 8216B1, Kitzlochklamm Klammkalk. (d) Quartz grains in sample 8286D1, Kitzlochklamm Klammkalk.

steinklamm have the appearance of a sheared mudstone, with numerous brittle faults dissecting the fine-grained host rock. Brittle fault intensity decreases away from the fault contact until a block and matrix mélange structure is attained at a distance of ~300 m.

[13] The Klammkalk unit at Lichtensteinklamm is pervasively veined, although the difficulty of accessing riverbed exposures at Lichtensteinklamm makes it difficult to compare deformation between the two Klamms. However, outcrops along a walkway carved into the gorge wall have a weakly developed S-C fabric, as at Kitzlochklamm. We infer that the weakness of this fabric is due to the lack of platy minerals within the Klammkalk. C-surfaces are broadly parallel to the Salzachtal fault, with one set dipping steeply north to northwest, and a smaller population dipping steeply north-northeast and south-southwest (Figure 4d). In contrast, the Klammkalk within ~20 m of the gouged Grauwacken zone contains a strong subvertical, fault-parallel foliation with fault-parallel veins. The contact between the well-foliated Klammkalk and gouged Grauwacken zone is not exposed.

4. Optical Microstructures

[14] The exposure of the SEMP at Kitzlochklamm allows us to directly observe how strain is partitioned just below, or within the lower part of, the brittle-ductile transition. Although the first-order observation at both the map and outcrop scales is that the majority of strain is localized along the pronounced, sharp contact between the Klammkalk and Grauwacken zone, indicating extreme strain localization, rocks throughout Kitzlochklamm exhibit ductile deformation fabrics consistent with the transport direction of the fault. To constrain the magnitude of this secondary, off-fault deformation, we evaluated grain-scale deformation throughout the outcrop by analyzing representative samples of the three major units present at Kitzlochklamm: Klammkalk, graphite-rich Grauwacken zone, and nongraphitic Grauwacken zone. We also compared grain-scale deformation in the Klammkalk at Kitzlochklamm and Lichtensteinklamm to see how deformation mechanisms changed below the depth of gouge formation. We did not conduct a similar analysis of the Grauwacken zone rocks, as those rocks closest to the fault at Lichtensteinklamm consist of clay gouge unsuitable for this type of microstructural analysis.

4.1. Kitzlochklamm Klammkalk

[15] The Klammkalk at Kitzlochklamm is a fine-grained marble tectonite, composed primarily of calcite grains 10–40 microns in diameter with axial ratios of 2:1, embedded in a matrix of equant calcite grains < 5 microns in diameter (Figure 7a). Vein calcite is larger, up to 1 mm in diameter. Most samples also contain local, thin (1–2 micron) solution seams parallel to the macroscopic foliation.

[16] The coarse-grained vein calcite displays twin intensities in the range 50–60 twins/mm. Twin widths are typically

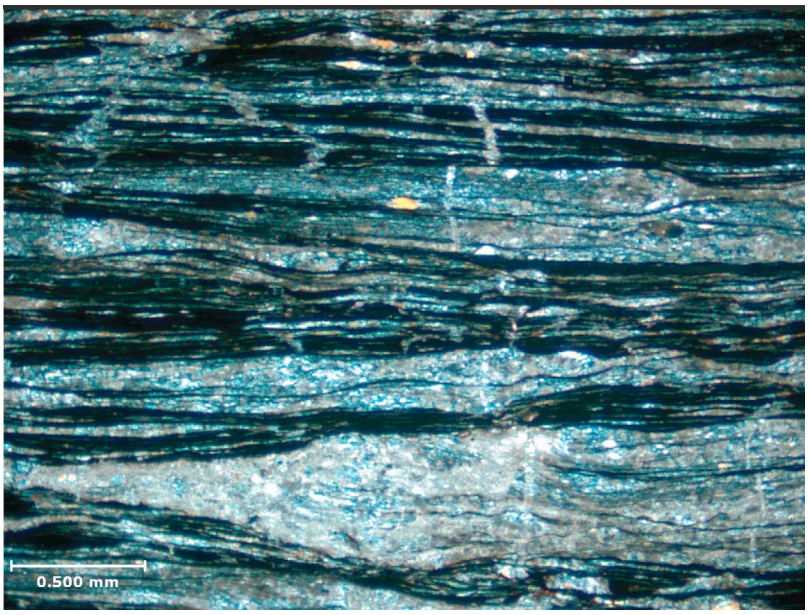

Figure 8. Representative section of sample 5812G35, Grauwacken zone graphite-rich schist from Kitzlochklamm. Veins are shortened and rotated into parallelism with the foliation, and pressure solution seams are abundant.

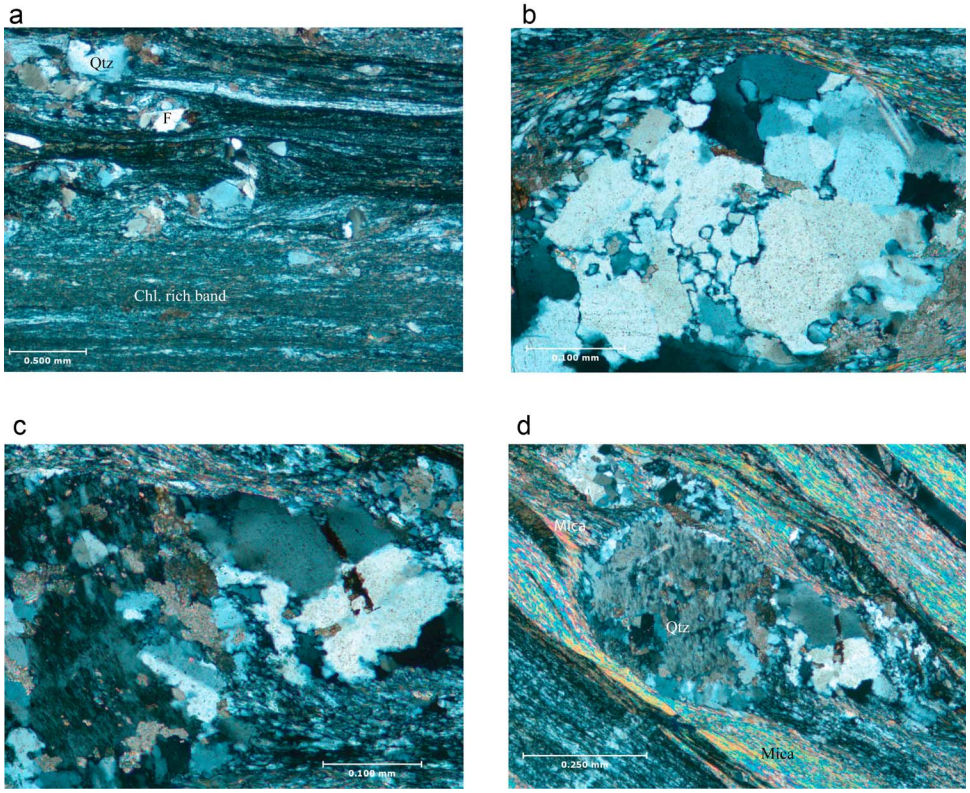

Figure 9. (a) The Grauwacken zone mica schist at Kitzlochklamm (sample 589G3) is composed of varying amounts of quartz, mica, feldspar, calcite, and chlorite. (b) Quartz in sample 589G3 displays lobate grain boundaries indicative of regime 1 bulge recrystallization. (c) Quartz in sample NOFG3, also from the Grauwacken zone mica schist at Kitzlochklamm, displays lobate grain boundaries and large subgrains. (d) Mica neoblasts in quartz strain shadow, sample 589G3.

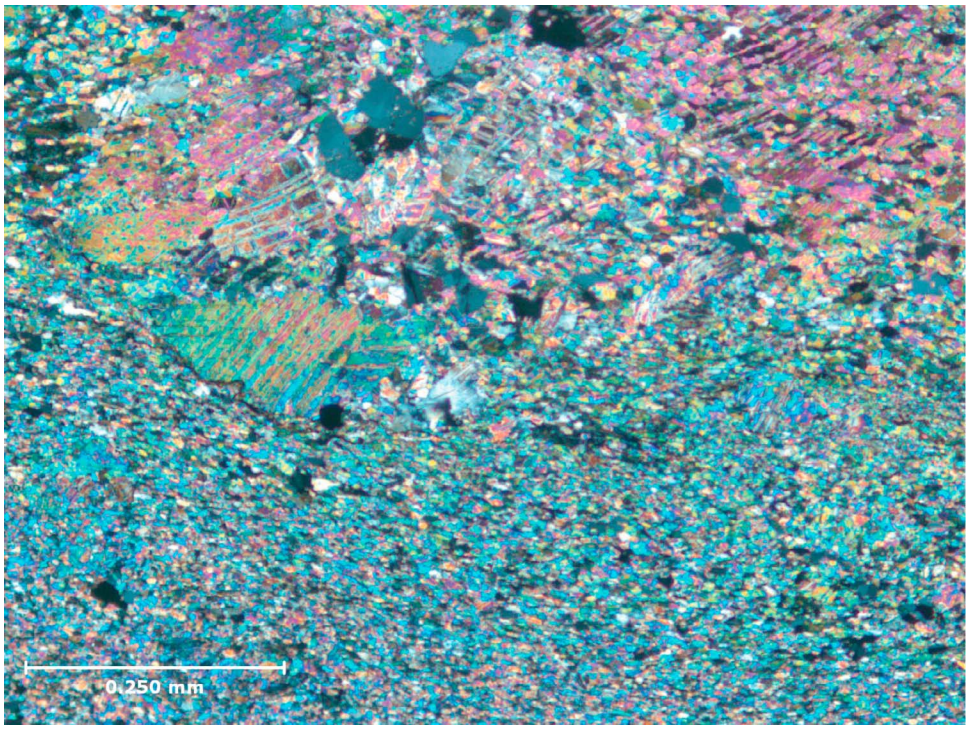

Figure 10. Sample 9106A1, Lichtensteinklamm Klammkalk, showing many microstructural similarities to the Klammkalk at Kitzlochklamm. Differences are primarily seen in calcite twin morphology: samples taken from Lichtensteinklamm tend to contain thinner twins at higher twin intensities, and type 4 recrystallized twins are observed much less often.

~2–4 microns, although some grains contain twin sets that are too thin to measure. The thick twins are commonly curved, tapered, and/or dynamically recrystallized (Figure 7b), typical of type 3 and 4 twins [*Ferrill et al.*, 2004]. Twins are less common in grains 10–40 microns in diameter; twins in such grains tend to be thick and tabular (type 4). The ultrafine matrix calcite appears to have been recrystallized via grain-boundary bulging.

[17] Quartz grains compose up to 20% of the samples. Grain size varies greatly, from 10 to 50 microns (Figures 7c and 7d). The quartz grains exhibit inhomogeneous flattening, irregular undulatory extinction, lobate grain boundaries, and large subgrains, all indicative of regime 1 bulging recrystallization [*Hirth and Tullis*, 1992].

4.2. Kitzlochklamm Grauwacken Graphite Schist

[18] The graphite schist is primarily composed of quartz, calcite, and feldspar layered between numerous solution seams (Figure 8). Calcite veins are heavily twinned. Rare quartz porphyroclasts up to 100 microns in diameter exhibit sweeping undulatory extinction, however, the majority of the quartz grains in these samples are 10–50 microns in diameter, with axial ratios of up to 4:1.

[19] Of all the lithologies that comprise the Grauwacken zone at Kitzlochklamm, the graphite schist shows the most evidence for diffusion creep. Graphite, micas, and other insoluble residues are concentrated along numerous (~20–30/mm), thick (~50 micron) solution seams parallel to the foliation. Further evidence of shortening includes vein fragments that have been truncated and rotated into the foliation.

4.3. Kitzlochklamm Grauwacken Nongraphite Schist

[20] The graphite-poor units of the Grauwacken zone, which include calcite schist, chlorite schist, and mica schist, all display similar microstructures (Figure 9). Quartz grains vary in diameter from 10 to 100 microns, with irregular to sweeping undulatory extinction. The most heavily recrystallized samples (from the mica schist) also exhibit large quartz subgrains (on par with the size of recrystallized quartz grains) and lobate grain boundaries (Figures 9b and 9c). Calcite is mostly 10–50 microns in diameter, although vein calcite grains are up to 200 microns in diameter. Whereas twins are generally difficult to observe in the fine-grained matrix calcite, some grains do contain type 1 and 2 twins [*Ferrill et al.*, 2004]. The coarser vein calcite contains thick (2–4 microns), bent twins, typical of type 3 twins [*Ferrill et al.*, 2004]. Feldspar is fractured in all samples, with some twins in the mica schist. All rocks have experienced solution mass transfer to varying degrees, as shown by offset and shortened veins, solution seams, and in the case of the mica schist, mica neoblasts in quartz strain shadows (Figure 9d).

4.4. Lichtenstein Klammkalk Samples

[21] The Klammkalk at Lichtensteinklamm shares many microstructures with the Kitzlochklamm Klammkalk. Specifically, at Lichtensteinklamm, most of the calcite grains

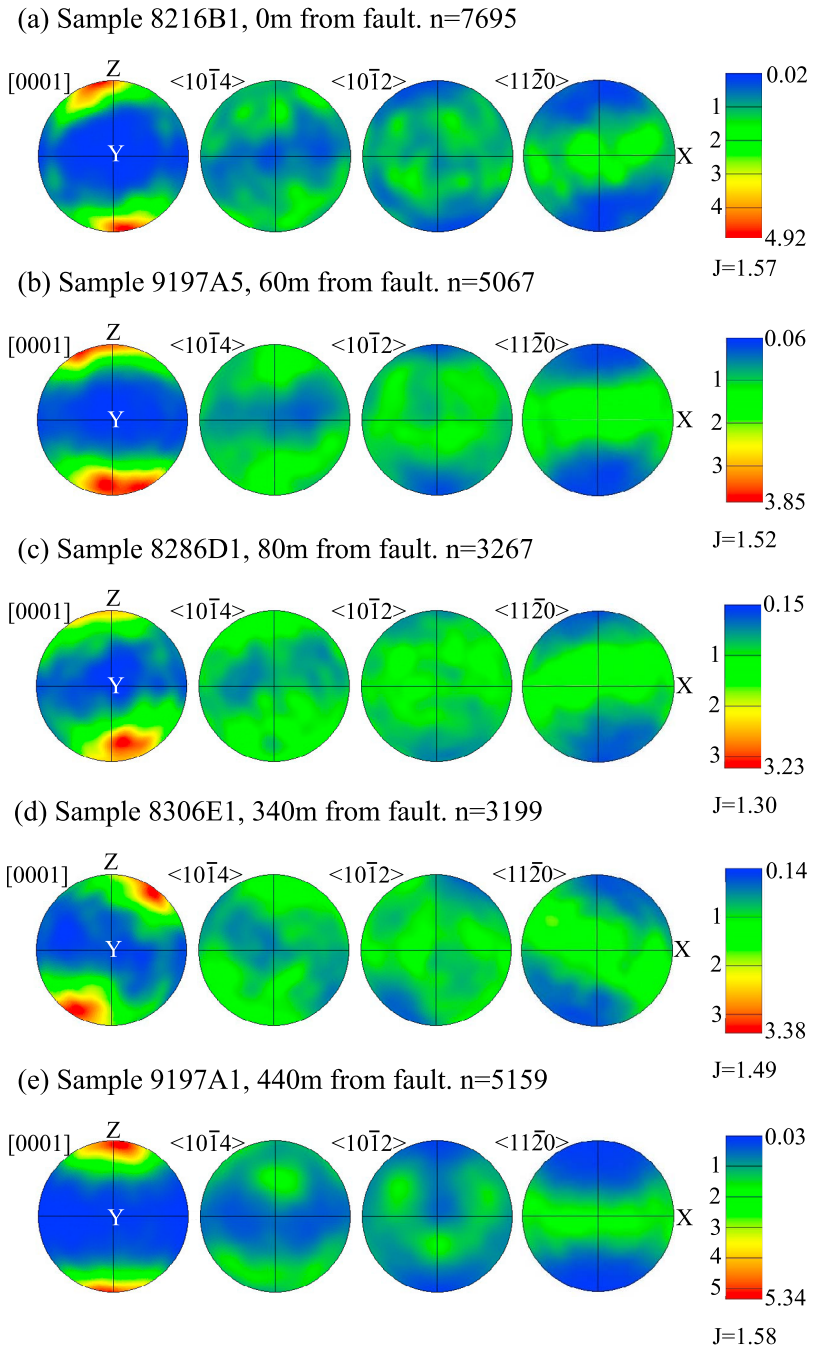

Figure 11. (a–e) Lattice-preferred orientations (LPOs) of calcite grains in samples of Kitzlochklamm Klammkalk taken along a fault-normal transect. All samples show the D3 fabric typical of shear zones bordering the Tauern Window [*Kurz et al.*, 2000]. The strength of this fabric, represented by both J and multiples of uniform distribution (MUD), is nearly constant along our 450 m long transect. LPOs here and in Figures 12–15 are lower hemisphere, equal-angle projections of one point per grain; crystallographic directions are plotted as poles to planes, avoiding the need for separate upper hemisphere projections; and the *X*, *Y*, and *Z* directions are defined by the samples' lineation and foliation.

vary from 10 to 40 microns in diameter with axial ratios of 2:1. Local lenses of ultra-fine-grained calcite contain grains <5 microns in diameter, whereas the largest vein calcite grains are up to 500 microns in diameter (Figure 10). Twins are most apparent in the coarse-grained vein calcite. Twins are typically thinner than at Kitzlochklamm, reaching a maximum of 2 microns. The thicker twins are generally tapered and curved, but lack recrystallized grains, and are therefore typical of type 2 and 3 twins [*Ferrill et al.*, 2004]. Twin intensities are in the range of 100–300 twins/mm.

[22] Quartz composes up to 25% of the Lichtensteinklamm Klammkalk samples, with most grains between 10 and 100 microns in diameter. These grains exhibit irregular to sweeping undulatory extinction; smaller grains

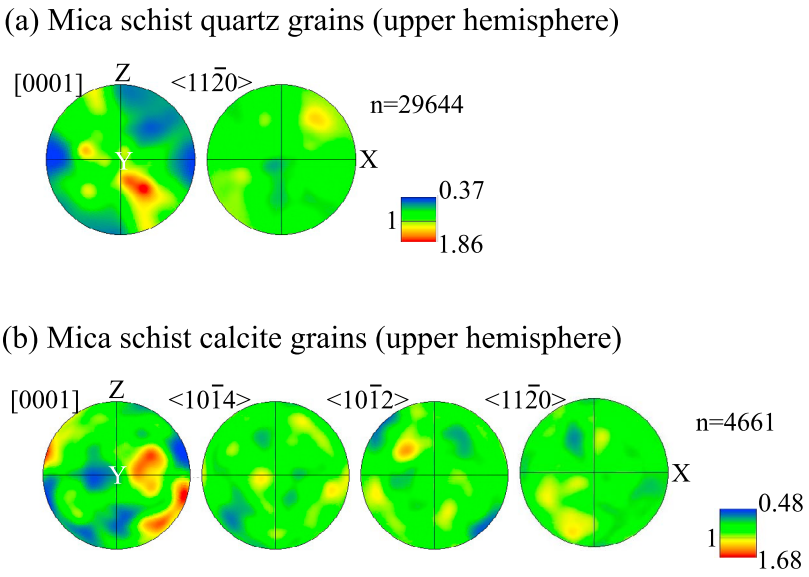

Figure 12. (a) LPOs of quartz grains from the Grauwacken zone mica schist (sample NOFG3): a diffuse, oblique girdle of [c] axes. The weak strength of this LPO suggests only minor dislocation creep in the mica schist quartz grains. (b) Random LPOs in calcite.

commonly have lobate grain boundaries. Solution seams are more common and are thicker than in Kitzlochklamm.

5. Electron Backscatter Diffraction

[23] In addition to analyzing the optical microstructures of samples taken from each Klamm, we used electron backscatter diffraction (EBSD) to provide further information on the deformation mechanisms operating in these outcrops. Low-resolution maps made of points spaced at about the grain scale were collected on an FEI Q400 field-emission scanning electron microscope at UCSB and indexed using Channel-5 HKL software, yielding lattice-preferred orientations (LPOs) of specific mineral phases in each slide. These data allow us to determine the relative importance of dislocation creep versus diffusion creep in the various units of the Klamms.

5.1. Kitzlochklamm Klammkalk

[24] We analyzed five samples spanning a 450 m fault-perpendicular distance within the Klammkalk. The goal of these analyses was to determine whether significant strain had occurred within the wall rocks on the southern side of the Salzachtal fault. Previous studies of ductile calcite from similar metamorphic conditions along the Helvetic Morcles nappe of Switzerland have documented a marked increase in LPO strength within meters of the fault [*Ebert et al.*, 2007; *Austin et al.*, 2008], reflecting the width over which strain was distributed within that ductile shear zone.

[25] All Klammkalk samples along our transect (Figure 11) yielded the "D3" fabric typical of shear zones bordering the Tauern Window [*Kurz et al.*, 2000]. Calcite [c] axes [0001] are clustered near Z, whereas ⟨a⟩ axes ⟨11–20⟩ are distributed along a girdle within the X-Y plane, representing fault-normal shortening [e.g., *Wang and Neubauer*, 1998]. This kind of fabric is known as a "deformation LPO," representing deformation at low temperatures prior to recrystallization [*Behrmann*, 1983; *Dietrich and Song*, 1984; *Schmid*, 1997; *Ratschbacher et al.*, 1991c; *Pieri et al.*, 2001a, 2001b; *Barnhoorn et al.*, 2004]. The strength of this fabric, represented by both the texture index J (calculated with the PFch5 software by D. Mainprice, 2005, available at ftp://www.gm.univ-montp2.fr/mainprice/CareWare_Unicef_Programs/) and multiples of uniform distribution (MUD; calculated in Channel-5), is nearly constant throughout our 450 m long transect. Most samples exhibited a MUD between 3 and 5, with a texture index J of ~1.5, which is relatively weak for rocks within a ductile shear zone associated with ~60 km of displacement.

5.2. Kitzlochklamm Grauwacken Zone

[26] Although solution transfer creep was clearly the dominant deformation mechanism operating in the graphite-rich schist of the Grauwacken zone, as shown by the extensive concentration of solution seams at all scales, the relative importance of dislocation and diffusion creep in the other Grauwacken units is difficult to determine from optical microstructures. To address this question, we analyzed representative samples of the mica schist and carbonate schist. Well-developed crystallographic fabrics indicate the importance of dislocation creep, whereas weak to random fabrics would point to diffusion creep as the dominant deformation mechanism [*Fliervoet et al.*, 1997]. In both the mica schist (sample NOFG3) and carbonate schist (sample G19b), we analyzed quartz and calcite grains. Feldspar clearly deformed via microcracking.

[27] Quartz grains in the Kitzlochklamm Grauwacken zone mica schist (Figure 12) have an LPO with a weak girdle of [c] axes, and a near-uniform distribution of ⟨a⟩ axes; the strength of this LPO is weak (MUD = 1.86). Calcite grains from the same unit have a similarly weak LPO (MUD = 1.68). In the Kitzlochklamm Grauwacken zone carbonate schist (Figure 13), the quartz grains have a slightly stronger LPO (MUD = 2.28), with a better-devel-

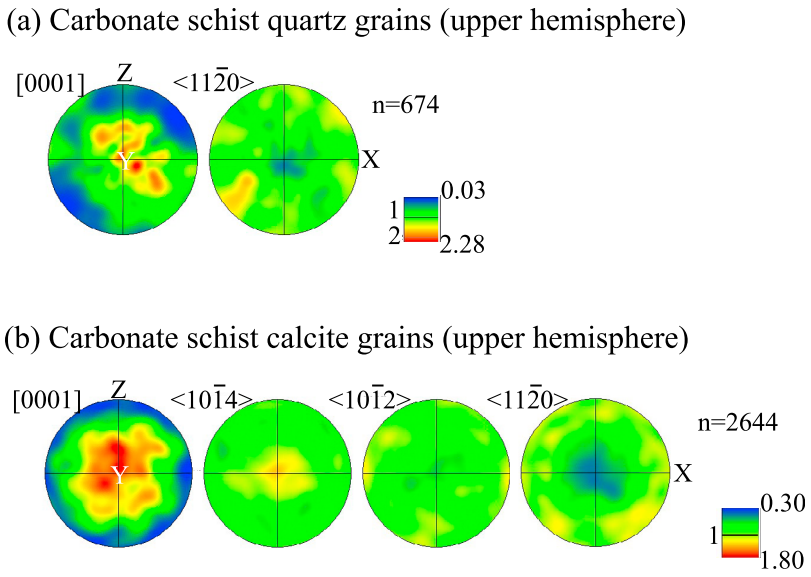

Figure 13. (a) LPOs of quartz grains from the Grauwacken zone carbonate schist form an oblique girdle of [c] axes. (b) Calcite grains exhibit a weak LPO.

oped girdle of [c] axes; the ⟨a⟩ axes are more diffuse. Calcite grains from the carbonate schist produce a random LPO (MUD = 1.8), as seen in the mica schist.

[28] Collectively, the weak to random LPOs observed in the mica and carbonate schist provide further evidence that the Grauwacken zone at Kitzlochklamm deformed primarily via solution transfer creep, accommodating fault-normal shortening.

5.3. Lichtensteinklamm Klammkalk

[29] Given the relative consistency of the fabrics at Kitzlochklamm, we analyzed only two samples of the Klammkalk at Lichtensteinklamm: one at a distance of 20 m to the fault, and the other at 50 m (Figure 14). As with Kitzlochklamm, these were "coarse" one-point-per-grain analyses designed to determine bulk calcite LPO. Both samples lack the D3 LPO observed in all Kitzlochklamm samples. The LPO strengths of MUD = 2.18 at 20 m and 1.51 at 50 m are weak.

6. Exhumation Depth: Raman Spectroscopy Results and Regional Considerations

[30] The Penninic units along the margins of the Tauern Window have greenschist-facies metamorphic minerals [*Genser et al.*, 1996], and our observations of ductile carbonate veins and shear bands in the Klamms, as well as ductile quartz and brittle feldspars, are consistent with this. Microstructural analysis of samples from both Klamms

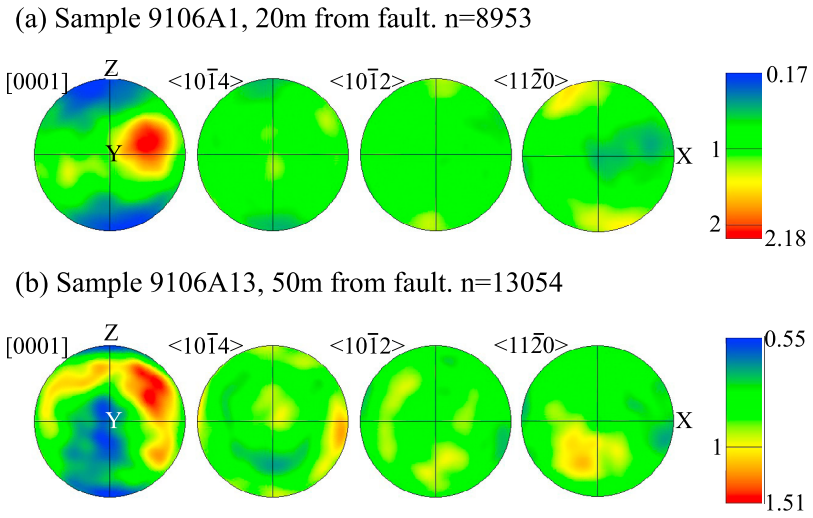

Figure 14. (a and b) Samples of Klammkalk taken at distances of 20 and 50 m from the SEMP at Lichtensteinklamm lack the "deformation LPO" we observe at Kitzlochklamm and that *Kurz et al.* [2000] documented in ductile shear zones bordering the Tauern Window.

indicates that Kitzlochklamm has been more deeply exhumed than Lichtensteinklamm. Specifically, twin morphologies from the Klammkalk are consistently indicative of higher-temperature deformation at Kitzlochklamm than at Lichtensteinklamm. Additionally, calcite from the Kitzlochklamm Klammkalk shows evidence for recrystallization via grain-boundary bulging, which is not observed in Lichtensteinklamm. Comparison of quartz in the same Klammkalk samples displays a similar pattern, with regime 1 bulging recrystallization evident at Kitzlochklamm but not at Lichtensteinklamm. Furthermore, calcite LPOs from Kitzlochklamm imply crystal plastic deformation throughout the Klammkalk, albeit at low strains, whereas the same unit at Lichtensteinklamm shows no evidence for the D3 fabric that has been documented at shear zones bordering the Tauern Window [*Kurz et al.*, 2000]. Together, these microstructural data suggest increasing dislocation and diffusion creep at the expense of cataclasis at the more deeply exhumed Kitzlochklamm outcrop.

[31] The exhumation depth of the SEMP in this region has not been quantified, as the marbles and schists at these outcrops are unsuitable for thermobarometry. However, the large amount of carbonaceous material (CM) in these rocks allowed us to constrain the peak metamorphic temperature using Raman spectroscopy [*Beyssac et al.*, 2002; *Rahl et al.*, 2005]. We conducted laser Raman measurements of CM in four polished thin sections, one from each side of the fault at each Klamm. Approximately 10 spot analyses were conducted for each thin section, depending on the prevalence of CM. The peak positions, band areas, and band heights of the D1, D2, and G bands for each analysis were determined with the program PeakFit 4.12 (Systat Software Inc.). These band areas and widths were then used to calculate peak metamorphic temperature for each spot analysis according to [*Beyssac et al.*, 2002]

$$T(^\circ C) = -445\ R2 + 641, \quad (1)$$

where $R2$ represents the relative areas of the $D1$, $D2$, and G bands:

$$R2 = D1/(G + D1 + D2). \quad (2)$$

The samples from Kitzlochklamm yield average temperatures of 380°C in the Grauwacken zone and 406°C in the Klammkalk. Samples from Lichtensteinklamm yielded temperatures of 435°C in the Grauwacken zone and 406°C in the Klammkalk. The uncertainty for these estimates is ±50°C over the temperature range 330–650°C on the basis of the dispersion of the points used by *Beyssac et al.* [2002] for calibration of the thermometer.

[32] When taking the uncertainty on these temperatures into consideration, some of our samples appear to be very close to the lower limit of the thermometer devised by *Beyssac et al.* [2002]. We therefore also calculated the temperature for each sample using the thermometer devised by *Rahl et al.* [2005], which can estimate peak metamorphic temperatures down to 100°C:

$$T(^\circ C) = 737.3 + 320.9\,R1 - 1067\,R2 - 80.638\,R1^2, \quad (3)$$

where $R2$ relates band areas as defined as above and $R1$ relates band heights according to

$$R1 = D1/G. \quad (4)$$

The samples from Kitzlochklamm yield average temperatures of 395°C in the Grauwacken zone and 445°C in the Klammkalk. Samples from Lichtensteinklamm yielded temperatures of 456°C in the Grauwacken zone and 390°C in the Klammkalk. These calculations predict peak metamorphic temperature to ±50°C at the 95% confidence level [*Rahl et al.*, 2005].

[33] On the basis of both sets of calculations, the rocks at both Klamms appear to have experienced peak temperatures around or just above 400°C. In general, these temperatures are consistent with the microstructural observations of dislocation creep in quartz and fully brittle deformation in feldspar, suggesting that the peak temperatures recorded by Raman spectroscopy are not significantly hotter than the temperatures experienced during fault slip. However, we should note that Raman spectroscopy is based on the irreversible conversion of CM to graphite, leaving open the possibility that these temperatures are related to an older metamorphism.

[34] We can use previous studies of exhumation along the SEMP to further constrain exhumation at the Klamms. Sixty kilometers to the west, the Rinderkarsee shear zone southeast of Krimml is a more deeply exhumed part of the Salzachtal fault (Figure 15). *Cole et al.* [2007] estimated that this shear zone has been exhumed from ~16–17 km depth. Where the SEMP terminates in the Vienna basin, some 300 km to the east of Krimml, the fault has experienced no exhumation [*Ratschbacher et al.*, 1991a, 1991b]. If the lateral exhumation gradient along the SEMP is constant along strike, the fault has been tilted up to the west by ~3° along strike. If correct, this would result in a very small difference in exhumation between the closely spaced Klamm outcrops. The fact that both Klamms produce very similar peak temperatures, combined with this simple geometric argument, suggests that the 18 km along-strike separation between the Klamms represents a relatively small difference in exhumation depth on the order of only ~1 km. We note, however, that regional tilt may not be constant along strike, and the exhumation gradient between the Klamms may have been steeper than the regional average, leaving open the possibility that the difference in exhumation may be >1 km. However, the similarity in peak metamorphic temperature and close proximity of these outcrops suggests a small difference in exhumation depth.

7. Discussion

[35] Our structural analyses indicate that the differentially exhumed Klamms span the brittle-ductile transition of the Salzachtal fault, with dominantly brittle deformation observed at Lichtensteinklamm, and dominantly ductile deformational fabrics observed at the more deeply exhumed Kitzlochklamm outcrop. Study of the fault zone rocks at each outcrop further suggests that at these depths, strain was highly localized along a narrow fault interface throughout the ~1 km depth range of the brittle-ductile transition exposed in the Klamms, with relatively minor distributed

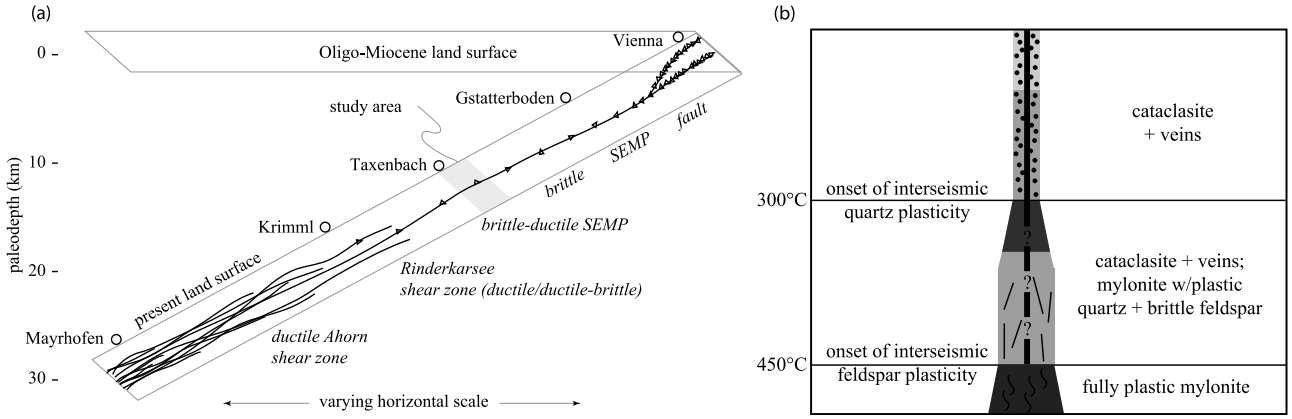

Figure 15. (a) Schematic reconstruction of the SEMP fault system during Oligo-Miocene time [after *Cole et al.*, 2007] compared against (b) a generalized shear zone model [after *Scholz*, 1988]. At our study sites near the brittle-ductile transition at Taxenbach, we observe the SEMP to be highly localized at outcrops that are both dominantly brittle (Lichtensteinklamm) and dominantly ductile (Kitzlochklamm). Our study at the more shallowly exhumed Gstatterboden outcrop found the majority of strain to be localized within a 10–40 m wide brittle core [*Frost et al.*, 2009], while *Cole et al.* [2007] found the more deeply exhumed Rinderkarsee shear zone had concentrated SEMP-related strain within a 100 m wide ductile/ductile-brittle shear zone. The SEMP reaches its greatest width in the Ahorn shear zone, where strain has been distributed within a 2 km wide mylonite belt [*Rosenberg and Schneider*, 2008]. Our results at the SEMP suggest that faults may not necessarily widen significantly concurrent with quartz ductility, as suggested by the model of *Scholz* [2002].

strain in the wall rocks. Specifically, our data reveal a ~70 m wide brittle high-strain fault core at Lichtensteinklamm that extends for ~20 m into the Klammkalk and ~50 m into the Grauwacken zone rocks. Although Grauwacken zone rocks to the north exhibit a pervasive shear fabric out to several hundred meters from the fault, the presence of a wide, well-developed gouge zone indicates extreme localization of most of the strain to a narrow zone adjacent to the main fault contact. Furthermore, EBSD analysis of the Klammkalk sampled adjacent to the 20 m wide higher-strain Klammkalk adjacent to the fault core shows only minor amounts of ductile strain. Conversely, we find abundant evidence of ductile deformation (including sheared and boudinaged veins, S-C fabrics) present in both the Klammkalk and Grauwacken zone units adjacent to the fault at Kitzlochklamm, with sub-vertical shear zones consistent with the orientation of the Salzachtal fault throughout the Grauwacken zone. However, the presence of heavily damaged graphite schist within centimeters of the sharply defined fault contact, combined with weak calcite fabrics observed in EBSD throughout the Klammkalk, points to a very narrow zone of strain accommodation at Kitzlochklamm.

[36] Our interpretation of data from Lichtensteinklamm is consistent with the notion that fault strength is primarily governed by frictional strength even at temperatures above 300°C, as suggested in the fault zone model of *Scholz* [2002]. This is supported by the lack of a well-developed LPO in the Klammkalk unit, combined with a wide, well-developed gouge zone displaying left-lateral Riedel shears adjacent to the fault contact. Furthermore, Grauwacken outcrops in the parking lots north of the gouge zone do not display the ductile shear fabrics evident at Kitzlochklamm, but rather have the appearance of a brittly sheared mudstone, with shear bounded, decimeter- to meter-scale phacoids of coarser-grained beds.

[37] A markedly different, more ductile style of deformation is observed at the more deeply exhumed Kitzlochklamm outcrop. The Grauwacken zone at this outcrop is characterized by a well-developed S-C fabric, and calcite grains in the Klammkalk produce the D3 fabric typical of ductile shear zones bordering the Tauern Window [*Kurz et al.*, 2000]. No evidence of gouge is found at the fault contact, although graphite schist adjacent to the fault has been heavily damaged. Together, these observations suggest a transition from dominantly brittle to dominantly ductile deformation over a relatively narrow depth range.

[38] The fact that Kitzlochklamm lacks either a gouge zone, as at Lichtensteinklamm, or a high-strain mylonitic core, is puzzling. The intense damage adjacent to the main fault contact, together with clear evidence for significant slip on the brittle faults bounding the 5 m wide fault sliver of Klammkalk 30 m into the Grauwacken zone, suggests that a significant component of slip at Kitzlochklamm may have been accommodated by brittle faulting. This may reflect hybrid behavior of the fault over individual earthquake cycles, with interseismic ductile deformation and coseismic localization of slip on brittle faults that extend down into the nominally ductile regime during seismic slip [e.g., *Sibson*, 1980]. Such behavior has been demonstrated for some recent large earthquakes. For example, *Hearn and Bürgmann* [2005] demonstrated that coseismic slip in the 1999 M 7.5 Izmit earthquake extended down to at least 20 km, in a region background microseismicity extends down to only ~16–17 km [e.g., *Bulut et al.*, 2007, 2009]. This requires that coseismic rupture extended below the "seismogenic zone" into velocity-strengthening material (albeit

probably weakly velocity strengthening, as the presence of strongly velocity-strengthening rocks would inhibit downward rupture) [*Hearn and Bürgmann*, 2005; *Hearn et al.*, 2009]. These observations are also consistent with coseismic deepening, and subsequent interseismic shallowing, of the maximum depth of aftershocks documented in some large earthquakes [e.g., *Rolandone et al.*, 2004].

[39] We did not see any evidence for pseudotachylites, which might be expected to form in such an environment, but pseudotachylites are commonly difficult to discern in the field. An alternative possibility is that either a high-strain mylonite or a brittle gouge zone formed at the lithologic contact, and has subsequently been faulted out. However, we see no evidence for even slivers of mylonite at either outcrop, and we do not observe any remnant evidence for extensive gouge development at Kitzlochklamm.

8. Conclusions

[40] Structural analysis of two fault-perpendicular transects along the exhumed Oligo-Miocene Salzachtal fault reveal highly localized strain throughout the brittle-ductile transition. Although there is minor distributed ductile deformation in the wall rocks at both study sites in the Klammkalk exposed on the south side of the fault, these fabrics are weak at Kitzlochklamm and absent at more than a few decimeters from the fault at Lichtensteinklamm. At Lichtensteinklamm, the presence of a 50 m wide, vertically foliated gouge zone at the main fault contact suggests highly localized slip. The Grauwacken zone rocks north of the fault at Kitzlochklamm preserve evidence for a wider zone of deformation, up to several hundred meters, but the ductile component of deformation in these rocks was dominated by solution creep that accommodated fault-normal shortening, rather than sinistral shear. Weak LPOs observed by EBSD indicate that little off-fault strain was accommodated by dislocation creep in these rocks. These results demonstrate that as deformation along the SEMP transitioned downward from dominantly brittle to dominantly ductile, strain remained localized, rather than broadening into a wide zone of distributed deformation.

[41] **Acknowledgments.** This research was funded by the U.S. National Science Foundation grants EAR-0309542 and EAR-0309995. Many thanks to Joshua Cole, Nicholas Barth, Edgar Scheidewig, and Veronika Geissler for their invaluable assistance in the field. Mark Brandon and Sandra McLaren provided helpful reviews.

References

Austin, N., B. Evans, M. Herwegh, and A. Ebert (2008), Strain localization in the Morcles Nappe (Helvetic Alps, Switzerland), *Swiss J. Geosci.*, *101*, 341–360, doi:10.1007/s00015-008-1264-2.

Barnhoorn, A., M. Bystricky, L. Burlini, and K. Kunze (2004), The role of recrystallization on the deformation behavior of calcite rocks: Large strain torsion experiments on Carrara marble, *J. Struct. Geol.*, *26*(5), 885–903, doi:10.1016/j.jsg.2003.11.024.

Behrmann, J. H. (1983), Microstructure and fabric transitions in calcite tectonites from the Sierra Alhamilla (Spain), *Geol. Rundsch.*, *72*(2), 605–618, doi:10.1007/BF01822084.

Beyssac, O., B. Goff'e, C. Chopin, and J. N. Rouzaud (2002), Raman spectrum of carbonaceous material in metasediments: A new geothermometer, *J. Metamorph. Geol.*, *20*, 859–871, doi:10.1046/j.1525-1314.2002.00408.x.

Bickle, M. J., and C. J. Hawkesworth (1978), Deformation phases and the tectonic history of the eastern Alps, *Geol. Soc. Am. Bull.*, *89*(2), 293–306, doi:10.1130/0016-7606(1978)89<293:DPATTH>2.0.CO;2.

Brace, W. F., and D. L. Kohlstedt (1980), Limits on lithospheric stress imposed by laboratory experiments, *J. Geophys. Res.*, *85*, 6248–6252, doi:10.1029/JB085iB11p06248.

Bulut, F., M. Bohnhoff, M. Aktar, and G. Dresen (2007), Characterization of aftershock-fault plane orientations of the 1999 Izmit (Turkey) earthquake using high-resolution aftershock locations, *Geophys. Res. Lett.*, *34*, L20306, doi:10.1029/2007GL031154.

Bulut, F., M. Bohnhoff, W. L. Ellsworth, M. Aktar, and G. Dresen (2009), Microseismicity at the North Anatolian Fault in the Sea of Marmara offshore Istanbul, NW Turkey, *J. Geophys. Res.*, *114*, B09302, doi:10.1029/2008JB006244.

Carter, N. L., and S. H. Kirby (1978), Transient creep and semibrittle behavior of crystalline rocks, *Pure Appl. Geophys.*, *116*, 807–839, doi:10.1007/BF00876540.

Chester, F. M. (1995), A rheologic model for wet crust applied to strike-slip faults, *J. Geophys. Res.*, *100*, 13,033–13,044, doi:10.1029/95JB00313.

Cole, J., B. Hacker, L. Ratschbacher, J. Dolan, G. Seward, E. Frost, and W. Frank (2007), Localized ductile shear below the seismogenic zone: Structural analysis of an exhumed strike-slip fault, Austrian Alps, *J. Geophys. Res.*, *112*, B12304, doi:10.1029/2007JB004975.

Decker, K., H. Peresson, and P. Faupl (1994), Miocene tectonics in the eastern Limestone Alps: Kinematics, paleostress and distribution of deformation during the lateral extrusion of the Central Alps, *Jahrb. Geol. Bundesanst.*, *137*, 5–18.

Dietrich, D., and H. Song (1984), Calcite fabrics in a natural shear environment: The Helvetic nappes of western Switzerland, *J. Struct. Geol.*, *6*(1–2), 19–32, doi:10.1016/0191-8141(84)90080-4.

Ebert, E., M. Herwegh, and A. Pfiffner (2007), Cooling induced strain localization in carbonate mylonites within a large-scale shear zones (Glarus thrust, Switzerland), *J. Struct. Geol.*, *29*(7), 1164–1184, doi:10.1016/j.jsg.2007.03.007.

Exner, C. H. (1996), Leitgesteine und Tektonik in Phylliten bei Wagrain und Radstadt, *Jahrb. Geol. Bundesanst.*, *139*, 155–190.

Ferrill, D. A., A. P. Morris, M. A. Evans, M. Burkhard, R. H. Groshong, and C. M. Onasch (2004), Calcite twin morphology: A low-temperature deformation geothermometer, *J. Struct. Geol.*, *26*(8), 1521–1529, doi:10.1016/j.jsg.2003.11.028.

Fliervoet, T. F., S. H. White, and M. R. Drury (1997), Evidence for dominant grain-boundary sliding deformation in greenschist- and amphibolite-grade polymineralic ultramylonites from the Redbank Deformed Zone, Central Australia, *J. Struct. Geol.*, *19*(12), 1495–1520, doi:10.1016/S0191-8141(97)00076-X.

Frost, E., J. Dolan, C. Sammis, B. Hacker, J. Cole, and L. Ratschbacher (2009), Progressive strain localization in a major strike-slip fault exhumed from midseismogenic depths: Structural observations from the Salzach-Ennstal-Mariazell-Puchberg fault system, Austria, *J. Geophys. Res.*, *114*, B04406, doi:10.1029/2008JB005763.

Genser, J., J. van Wees, S. Cloetingh, and F. Neubauer (1996), Eastern Alpine tectono-metamorphic evolution: Constraints from two-dimensional P-T-t modeling, *Tectonics*, *15*(3), 584–604, doi:10.1029/95TC03289.

Hacker, B. R. (1997), Diagenesis and the fault-valve seismicity of crustal faults, *J. Geophys. Res.*, *102*, 24,459–24,467, doi:10.1029/97JB02025.

Hacker, B. R., and J. M. Christie (1990), Brittle/ductile and plastic/cataclastic transitions in experimentally deformed and metamorphosed amphibolite, in *The Brittle-Ductile Transition in Rocks*, *Geophys. Monogr. Ser.*, vol. 56, edited by A. G. Duba et al., pp. 127–147, AGU, Washington, D. C.

Hearn, E. H., and R. Bürgmann (2005), The effect of elastic layering on inversions of GPS data for earthquake slip and resulting stress changes, *Bull. Seismol. Soc. Am.*, *95*, 1637–1653, doi:10.1785/0120040158.

Hearn, E. H., S. McClusky, S. Ergintav, and R. E. Reilinger (2009), Izmit earthquake postseismic deformation and dynamics of the North Anatolian Fault Zone, *J. Geophys. Res.*, *114*, B08405, doi:10.1029/2008JB006026.

Hirth, G., and J. Tullis (1992), Dislocation creep regimes in quartz aggregates, *J. Struct. Geol.*, *14*(2), 145–159, doi:10.1016/0191-8141(92)90053-Y.

Hobbs, B. E., A. Ord, and C. Teyssier (1986), Earthquakes in the ductile regime?, *Pure Appl. Geophys.*, *124*(1–2), 309–336.

Janecke, S. U., and J. P. Evans (1988), Feldspar-influenced rock rheologies, *Geology*, *16*, 1064–1067, doi:10.1130/0091-7613(1988)016<1064:FIRR>2.3.CO;2.

Kurz, W., F. Neubauer, and J. Genser (1996), Kinematics of Penninic nappes (Glockner nappe and basement-cover nappes) in the Tauern Window (eastern Alps, Austria) during subduction and Penninic-Austroalpine collision, *Eclogae Geol. Helv.*, *89*, 573–605.

Kurz, W., F. Neubauer, W. Unzog, J. Genser, and X. Wang (2000), Microstructural and textural development of calcite marbles during polyphase

deformation of Penninic units within the Tauern Window (Eastern Alps), *Tectonophysics*, *316*, 327–342, doi:10.1016/S0040-1951(99)00257-7.

Lin, A., S. Maruyama, A. Stallard, K. Michibayashi, A. Camacho, and K. Kano (2005), Propagation of seismic slip from brittle to ductile crust: Evidence from pseudotachylyte of the Woodroffe thrust, central Australia, *Tectonophysics*, *402*, 21–35, doi:10.1016/j.tecto.2004.10.016.

Linzer, H. G., L. Ratschbacher, and W. Frisch (1995), Transpressional collision structures in the upper crust of the fold-thrust belt of the Northern Calcareous Alps, *Tectonophysics*, *242*, 41–61, doi:10.1016/0040-1951(94)00152-Y.

Linzer, H. G., F. Moser, R. Nemes, L. Ratschbacher, and B. Sperner (1997), Build-up and dismemberment of a classical fold-and-thrust belt: From non-cylindrical stacking to lateral extrusion in the eastern Northern Calcareous Alps, *Tectonophysics*, *272*, 97–124, doi:10.1016/S0040-1951(96)00254-5.

Linzer, H. G., K. Decker, H. Peresson, R. Dell'Mour, and W. Frisch (2002), Balancing orogenic float of the Eastern Alps, *Tectonophysics*, *354*, 211–237, doi:10.1016/S0040-1951(02)00337-2.

Montesi, L. G. J., and G. Hirth (2003), Grain size evolution and the rheology of ductile shear zones: From laboratory experiments to postseismic creep, *Earth Planet. Sci. Lett.*, *211*(1–2), 97–110, doi:10.1016/S0012-821X(03)00196-1.

Passchier, C. W. (1982), Pseudotachylyte and the development of ultramylonite bands in the Saint-Barthelemy Massif, French Pyrenees, *J. Struct. Geol.*, *4*(1), 69–79, doi:10.1016/0191-8141(82)90008-6.

Pestal, G., and E. Hejl (2005), *Geologische Karte von Salzburg*, vol. 1, scale 1:200,000, Geol. Bundesanst., Vienna, Austria.

Pieri, M., L. Burlini, K. Kunze, D. L. Olgaard, and I. C. Stretton (2001a), Rheological and microstructural evolution of Carrara marble with high shear strain: Results from high temperature torsion experiments, *J. Struct. Geol.*, *23*(9), 1393–1413, doi:10.1016/S0191-8141(01)00006-2.

Pieri, M., K. Kunze, L. Burlini, I. C. Stretton, D. L. Olgaard, J.-P. Burg, and H. R. Wenk (2001b), Texture development of calcite by deformation and dynamic recrystallization at 1000 K during torsion experiments of marble to large strains, *Tectonophysics*, *330*, 119–140, doi:10.1016/S0040-1951(00)00225-0.

Rahl, J. M., K. M. Anderson, M. T. Brandon, and C. Fassoulas (2005), Raman spectroscopic carbonaceous material thermometry of low-grade metamorphic rocks: Calibration and application to tectonic exhumation in Crete, Greece, *Earth Planet. Sci. Lett.*, *240*(2), 339–354, doi:10.1016/j.epsl.2005.09.055.

Ratschbacher, L., W. Frisch, H.-G. Linzer, and O. Merle (1991a), Lateral extrusion in the Eastern Alps: 2. Structural analysis, *Tectonics*, *10*(2), 257–271, doi:10.1029/90TC02623.

Ratschbacher, L., O. Merle, P. Davy, and P. Cobbold (1991b), Lateral extrusion in the Eastern Alps: 1. Boundary conditions and experiments scaled for gravity, *Tectonics*, *10*(2), 245–256, doi:10.1029/90TC02622.

Ratschbacher, L., H. R. Wenk, and M. Sintubin (1991c), Calcite textures: Examples from nappes with strain-history partitioning, *J. Struct. Geol.*, *13*(4), 369–384, doi:10.1016/0191-8141(91)90011-7.

Rolandone, F., R. Bürgmann, and R. M. Nadeau (2004), The evolution of the seismic-aseismic transition during the earthquake cycle: Constraints from the time-dependent depth distribution of aftershocks, *Geophys. Res. Lett.*, *31*, L23610, doi:10.1029/2004GL021379.

Rosenberg, C. L., and S. Schneider (2008), The western termination of the SEMP Fault (eastern Alps) and its bearing on the exhumation of the Tauern Window, in *Tectonic Aspects of the Alpine-Carpathian-Dinaride System*, *Geol. Soc. Spec. Publ.*, 298, 197–218, doi:10.1144/SP298.10.

Rutter, E. H. (1986), On the nomenclature of mode of failure transitions in rocks, *Tectonophysics*, *122*, 381–387.

Schmid, J. (1997), The genesis of white marbles: Geological cause and archaeological applications, Ph.D. thesis, 156 pp., Univ. of Bern, Bern.

Scholz, C. H. (1988), The brittle-plastic transition and the depth of seismic faulting, *Geol. Rundsch.*, *77*(1), 319–328, doi:10.1007/BF01848693.

Scholz, C. H. (2002), *The Mechanics of Earthquakes and Faulting*, 471 pp., Cambridge Univ. Press, New York.

Shigematsu, N., K. Fujimoto, T. Ohtani, and K. Goto (2004), Ductile fracture of fine grained plagioclase in the brittle-plastic transition regime: Implication for earthquake source nucleation, *Earth Planet. Sci. Lett.*, *222*(3–4), 1007–1022.

Shimamoto, T. (1989), The origin of S-C mylonites and a new fault-zone model, *J. Struct. Geol.*, *11*(1–2), 51–64, doi:10.1016/0191-8141(89)90035-7.

Sibson, R. (1980), Transient discontinuities in ductile shear zones, *J. Struct. Geol.*, *2*(1–2), 165–171, doi:10.1016/0191-8141(80)90047-4.

Sibson, R. H. (1982), Fault zone models, heat flow, and the depth distribution of earthquakes in the continental crust of the United States, *Bull. Seismol. Soc. Am.*, *72*, 151–163.

Sibson, R. H. (1984), Roughness at the base of the seismogenic zone: Contributing factors, *J. Geophys. Res.*, *89*, 5791–5799, doi:10.1029/JB089iB07p05791.

Tullis, J., and R. A. Yund (1977), Experimental deformation of dry Westerly Granite, *J. Geophys. Res.*, *82*, 5705–5718, doi:10.1029/JB082i036p05705.

Tullis, J., and R. A. Yund (1992), The brittle-ductile transition in feldspar aggregates: An experimental study, in *Fault Mechanics and Transport Properties of Rocks*, edited by B. Evans and T.-F. Wong, pp. 89–117, doi:10.1016/S0074-6142(08)62816-8, Academic, San Diego, Calif.

Wang, X., and F. Neubauer (1998), Orogen-parallel strike-slip faults bordering metamorphic core complexes: The Salzach-Enns fault zone in the Eastern Alps, Austria, *J. Struct. Geol.*, *20*(6), 799–818, doi:10.1016/S0191-8141(98)00013-3.

White, J. C. (1996), Transient discontinuities revisited: Pseudotachylyte, plastic instability and the influence of low pore fluid pressure on deformation processes in the mid-crust, *J. Struct. Geol.*, *18*(12), 1471–1477, doi:10.1016/S0191-8141(96)00059-4.

J. Dolan, Department of Earth Sciences, University of Southern California, 3651 Trousdale Pkwy., Los Angeles, CA 90089, USA.

E. Frost, Fugro William Lettis and Associates, 27220 Turnberry Ln., Ste. 110, Valencia, CA 91355, USA. (e.frost@fugro.com)

B. Hacker and G. Seward, Department of Earth Science, University of California, 1006 Webb Hall, MC 9630, Santa Barbara, CA 93106, USA.

L. Ratschbacher, Tektonophysik–Institut für Geowissenschaften, Technische Universität Bergakademie Freiberg, Bernhard-von-Cottastrasse 2, Freiberg D-09596, Germany.